Environmental Research 201 (2021) 111566

Contents lists available at ScienceDirect

Environmental Research

journal homepage: www.elsevier.com/locate/envres

Quantitative proteomic analysis of marine biofilms formed by filamentous cyanobacterium

M.J. Romeu [a,1], D. Domínguez-Pérez [b,1], D. Almeida [b], J. Morais [b], M.J. Araújo [b], H. Osório [c,d,e], A. Campos [b], V. Vasconcelos [b,f], F.J. Mergulhão [a,*]

[a] LEPABE, Laboratory for Process Engineering, Environment, Biotechnology and Energy, Faculty of Engineering, University of Porto, Rua Dr. Roberto Frias, 4200-465 Porto, Portugal
[b] CIIMAR, Interdisciplinary Centre of Marine and Environmental Research, University of Porto, Terminal de Cruzeiros do Porto de Leixões, Av. General Norton de Matos s/n, 4450-208, Matosinhos, Portugal
[c] i3S –Instituto de Investigação e Inovação em Saúde, Universidade do Porto, 4200-135, Porto, Portugal
[d] Institute of Molecular Pathology and Immunology of the University of Porto, IPATIMUP, Rua Júlio Amaral de Carvalho 45, 4200-135, Porto, Portugal
[e] Faculty of Medicine, University of Porto, Al. Prof. Hernâni Monteiro, 4200-319, Porto, Portugal
[f] Department of Biology, Faculty of Sciences, University of Porto, Rua do Campo Alegre, 4169-007, Porto, Portugal

ARTICLE INFO

Keywords:
Marine biofouling
Cyanobacterial biofilms
Shotgun proteomic
LC-MS/MS
Hydrodynamics
Fouling surfaces

ABSTRACT

Cyanobacterial molecular biology can identify pathways that affect the adhesion and settlement of biofouling organisms and, consequently, obtain novel antifouling strategies for marine applications. Proteomic analyses can provide an essential understanding of how cyanobacteria adapt to different environmental settings. However, only a few qualitative studies have been performed in some cyanobacterial strains. Considering the limited knowledge about protein expression in cyanobacteria in different growing conditions, a quantitative proteomic analysis by LC-MS/MS of biofilm cells from a filamentous strain was performed. Biofilms were also analysed through standard methodologies for following cyanobacterial biofilm development. Biofilms were formed on glass and perspex at two relevant hydrodynamic conditions for marine environments (average shear rates of 4 s^{-1} and 40 s^{-1}). Biofilm development was higher at 4 s^{-1} and no significant differences were found between surfaces. Proteomic analysis identified 546 proteins and 41 were differentially expressed. Differences in protein expression were more noticeable between biofilms formed on glass and perspex at 4 s^{-1}. When comparing biofilms formed on different surfaces, results suggest that biofilm development may be related to the expression of several proteins like a beta-propeller domain-containing protein, chaperone DnaK, SLH domain-containing proteins, an OMF family outer membrane protein, and/or additional uncharacterized proteins. Regarding the hydrodynamic effect, biofilm development can be related to SOD enzyme expression, to proteins related to photosynthetic processes and to a set of uncharacterized proteins with calcium binding domains, disordered proteins, and others involved in electron transfer activity. Studies that combine distinct approaches are essential for finding new targets for antibiofilm agents. The characterisation performed in this work provides new insights into how shear rate and surface affect cyanobacterial biofilm development and how cyanobacteria adapt to these different environmental settings from a macroscopic standpoint to a proteomics context.

1. Introduction

Marine biofouling has several economic, environmental, and ecological impacts (Bharti et al., 2017; Carvalho, 2018). Biofilms are a particular concern in aquaculture, heat exchangers, maritime transport, water desalination and the oil and gas industry. In biofilms, organisms cooperate and improve their chances of survival when subjected to harsh environmental conditions. Indeed, in marine environments, several parameters can affect the development of these biofilms, such as salt, nutrient and organic matter concentration, light access, pH,

* Corresponding author. LEPABE, Laboratory for Process Engineering, Environment, Biotechnology and Energy, Faculty of Engineering, University of Porto, Rua Dr. Roberto Frias, 4200-465, Porto, Portugal.
E-mail address: filipem@fe.up.pt (F.J. Mergulhão).
[1] These authors contributed equally to this work.

https://doi.org/10.1016/j.envres.2021.111566
Received 2 March 2021; Received in revised form 14 June 2021; Accepted 18 June 2021
Available online 25 June 2021
0013-9351/

temperature, hydrodynamic conditions, as well as the abiotic or biotic surface in which biofilm formation occurs (Carvalho, 2018). Cyanobacteria dominate marine and phototrophic biofilms and they have cosmopolitan distribution due to their inherent capacity to withstand various biotic and abiotic stresses. These microfouler organisms can also promote the adhesion of macrofouler organisms such barnacles, mussels, algae and seaweeds in aquatic environments (Mieszkin et al., 2013). Integration among several disciplines, such as genetics, biology, and chemistry, is essential for progress in marine biofilm research. Therefore, cyanobacterial molecular biology is an emerging field for further developments and improvements (Santos-Merino et al., 2019; Sun et al., 2018). Analyses of protein expression can provide an essential understanding of how cyanobacteria adapt to different environmental settings. It is crucial to study the protein expression level in different conditions, particularly in biofilms, since biofilm development under altered conditions may be associated with quantitative differences in their proteome. Therefore, quantitative proteomics studies allow establishing a relationship between the relative expression level of the identified proteins under different conditions. However, few proteomics studies address marine biofilms (Leary et al., 2014), and cyanobacteria data is scarce (Babele et al., 2019). Moreover, the small number of quantitative proteomic studies performed with filamentous cyanobacterium is restricted to *Anabaena, Nostoc,* and *Spirulina* cyanobacterial genus. These studies only analysed the impact of limited and specific parameters on protein expression, such as temperature (Kurdrid et al., 2011), salt (Wang et al., 2013) and arsenic stress (Pandey et al., 2012), ultraviolet-B light exposure (Babele et al., 2015), uranium tolerance (Panda et al., 2017) or N_2-fixing and non-N_2-fixing conditions (Ow et al., 2008). Different factors have been reported on cyanobacterial biofilm development, such as the involvement of the signaling molecule cyclic dimeric GMP (Agostoni et al., 2016; Enomoto et al., 2014), extracellular proteins (Oliveira et al., 2015; Parnasa et al., 2016; Zilliges et al., 2008) or type IV pili (Allen et al., 2019).

Identifying proteins expressed in a defined condition is a useful tool to understand the cellular response and to identify pathways that are activated or down-regulated under different circumstances to which cells were subjected (Battchikova et al., 2018; Muthusamy et al., 2017). Knowledge about protein expression under different biofilm development conditions is essential to clarify their role on biofilm phenotypes. These studies can help to identify pathways affecting adhesion and settlement of biofouling organisms and can lead to new targets for the development of novel antifouling strategies for marine applications.

The Blue Biotechnology and Ecotoxicology Culture Collection (LEGE-CC) is a biological resource center that comprises more than 1000 different cyanobacterial and microalgae strains (Ramos et al., 2018). The unidentified filamentous cyanobacterium LEGE 06007 strain was used in this study, given the relevance of cyanobacteria on marine biofouling. This strain has also shown good biofilm formation behavior during pre-screening of the collection. Although several biological and physico-chemical parameters have been identified as modulators of biofilm development, the fouling surface properties and flow velocity/shear rate have a critical impact on marine biofilms (Faria et al., 2020a, 2020b, 2021). Hence, the first goal of this study was to perform a biofouling potential evaluation of this marine cyanobacterium, which has recently been restructured on taxonomic level (Ramos et al., 2018). Previously included on *Phormidium* genus, after a revaluation of taxonomic assignments based on approaches that combine morphological and phylogenetic data, evaluation of its characteristics did not allow an unequivocal identification at the genus or order level. The second aim of this study was to perform a quantitative proteomics analysis of this cyanobacterium under different biofilm development conditions to establish a relationship between the relative expression level of the identified proteins under different settings (different hydrodynamic conditions and surfaces) and biofilm development. For this purpose, we performed a shotgun proteomic analysis of the digested peptides obtained from two distinct sample preparation methods – the Filter Aided Sample Preparation (FASP) (Wiśniewski et al., 2009), and the single-pot solid-phase-enhanced sample-preparation (SP3) protocol (Hughes et al., 2019). To the best of our knowledge, there are no quantitative proteomics studies evaluating the impact of different surfaces and different hydrodynamic conditions on cyanobacterial biofilm behavior. Therefore, this is the first work investigating the biofouling potential of this cyanobacterial strain and its proteome profile obtained from different biofilm development conditions by applying standard methodologies for biofilm development and a quantitative proteomics approach. Since the information on the molecular basis of these processes in cyanobacteria is scarce, the quantitative proteomic analysis carried out in this work is extremely relevant. Moreover, few studies have been performed in this research field addressing filamentous cyanobacterial biofilms.

2. Materials and methods

2.1. Organism and inocula preparation

Unidentified filamentous cyanobacterium LEGE 06007 was isolated from a wave-exposed rock in the intertidal zone at São Martinho do Porto beach, Portugal (39.50694 N 9.136311 W), and it was obtained from the LEGE-CC located at CIIMAR, Matosinhos, Portugal (Ramos et al., 2018). Cells were grown in 750 mL culture in Z8 medium (Kotai, 1972) supplemented with 25 g l^{-1} of synthetic sea salts (Tropic Marin) and B_{12} vitamin (Sigma Aldrich, Merck, Saint Louis, MO, USA), which supports the growth and cyanobacteria maintenance. The culture was performed under 14 h light (10–30 μmol photons m^{-2} s^{-1})/10 h dark cycles, at 25 °C.

2.2. Biofilm formation

Biofilm development was evaluated on agitated 12-well microtiter plates (VWR International, Carnaxide, Portugal), since this platform was shown to mimic the hydrodynamic conditions found in marine environments (Romeu et al., 2019). To assess the surface effect on protein expression, biofilms were developed on glass (Vidraria Lousada, Lda, Portugal) and perspex (Neves & Neves, Lda, Portugal) coupons (1 cm^2). These substrates have different hydrophobicity (Romeu et al., 2019) and they also represent commonly submerged artificial surfaces found on different equipment in aquatic and marine environments such as underwater windows of boats, aquaculture equipment, flotation spheres, moored buoys, underwater cameras, measuring devices or sensors (Taylor, 1996; Blain et al., 2004; King et al., 2006). Surface preparation and sterilisation was performed as previously described (Romeu et al., 2019). Before inoculation, the cyanobacterial suspension was adjusted to a chlorophyll *a* concentration of 1.5 μg ml^{-1}, since chlorophyll *a* concentration is commonly used as biomass indicator in aquatic environments. After 2 ml of cyanobacterial suspension were incubated for 24 h at 4 °C in the dark for a maximal chlorophyll *a* extraction, the samples were centrifuged at 3202 g, for 5 min at room temperature and the supernatant was transferred to a glass cuvette. The absorbance at 750 nm (turbidity), 665 nm (chlorophyll *a*) and 652 nm (chlorophyll *b*) was determined using a V-1200 spectrophotometer (VWR International China Co., Ltd, Shanghai, China). The chlorophyll *a* concentration was calculated through the following equation (Porra et al., 1989):

$$\text{Chl } a\ (\mu g.ml^{-1}) = 16.29 \times A^{665} - 8.54 \times A^{652} \quad (1)$$

These measurements were assessed in triplicate and dilutions were performed using Z8 medium supplemented with 25 g l^{-1} of synthetic sea salts and vitamin B_{12}. Thus, a volume of 3 ml of adjusted cyanobacterial suspension was inoculated in each well, in which coupons of each surface were previously fixed with transparent double-sided adhesive tape. To assess the effect of hydrodynamics on protein expression, cyanobacterial biofilm formation at different shear rates was tested. Although a shear rate of 50 s^{-1} has been reported for a ship in a harbour

(Bakker et al., 2003), equipment and devices which are in similar environments such as partially submerged or even moored equipment, as underwater cameras, flotation spheres, sensors, and even transparent hulls of boats or their windows are likely to be subjected to similar shear values (Romeu et al., 2019). Microtiter plates were incubated at 25 °C in an orbital shaker with a 25 mm orbital radius (Agitorb 200ICP, Norconcessus, Portugal) at 185 rpm, yielding average and maximum shear rates of 40 and 120 s^{-1}, respectively (Romeu et al., 2019). Moreover, it has been reported that lower fluid velocities (0.2 m s^{-1}) promote the growth of filamentous green algae and cyanobacteria (Flemming et al., 2009; Minchin and Gollasch, 2003) and that marine biofouling can be favoured at low shear rates (Faria et al., 2020a). Therefore, biofilm development was also assessed at lower shear rate conditions (average shear rate of 4 s^{-1}, reaching a maximum value of 11 s^{-1}, which are obtained in the same incubator at a shaking frequency of 40 rpm). Overall, these values of shear rate include different ranges that can be found in marine environments and which are important for marine biofouling. Biofilm development was followed for seven weeks (49 days) since it is accepted that a two-month interval for maintenance is the minimum duration for economically viable underwater monitoring systems, as previously reported (Blain et al., 2004; Romeu et al., 2019). During this incubation time, the medium was replaced twice a week. In order to mimic real light exposure periods, a photoperiod of 14 h light (8–10 μmol photons m^{-2} s^{-1})/10 h dark cycles) was applied (Romeu et al., 2019). This methodology, which has been used to assess the antifouling performance of different surfaces, was further validated by field tests as previously described (Silva et al., 2021).

2.3. Biofilm analysis

Although the initial stages of biofilm formation could be assessed by counting the number of adhered cells if a coccoid cyanobacterium was used (Faria et al., 2021), this study uses a filamentous cyanobacterial strain which precludes reliable determination of adhered cell numbers. Since preliminary studies have shown that seven days was the minimum time to obtain reliable and quantifiable results through the methods used in this work, biofilm analysis was performed every seven days, at which three coupons for each surface and hydrodynamic condition were analysed. To eliminate loosely attached cyanobacteria, the culture medium was carefully removed, and the wells were filled with 3 ml of sterile sodium chloride solution (8.5 g l^{-1}) (Romeu et al., 2019) to evaluate the cyanobacterial biofilms structure by Optical Coherence Tomography (OCT). In order to complement the characterization of cyanobacterial biofilms, the determination of their wet weight and chlorophyll *a* content was performed. Additionally, the crystal violet assay was performed for total biomass quantification.

2.3.1. Optical Coherence Tomography

Images from cyanobacterial biofilms developed on both surfaces and under the different hydrodynamic conditions were captured as reported in Romeu et al. (2019). For each coupon, 2-D imaging was performed with a minimum of three fields of view, to ensure the accuracy and reliability of the results obtained. Image analysis was performed using a routine developed in the Image Processing Toolbox from MATLAB 8.0 and Statistics Toolbox 8.1 (The MathWorks, Inc., Natick, Massachusetts, USA) as reported in Romeu et al. (2020). The mean biofilm thickness was calculated according to the following equation (2):

$$\overline{L}_F = \frac{1}{N} \sum_{i=1}^{N} L_{F,i} \quad (2)$$

where $L_{F,i}$ is a local biofilm thickness measurement at location *i*, *N* equals the number of thickness measurements and $\overline{L}_F$ is the mean biofilm thickness.

Biofilm roughness was analysed by determining the roughness coefficient because this parameter allows comparing the structure of different biofilms, across different studies and across scales once this value is normalized to the mean biofilm thickness (Romeu et al., 2019). The relative roughness coefficient (R_a^*) was calculated using the following equation, according to Wagner and Horn (2017):

$$R_a^* = \frac{1}{N} \sum_{i=1}^{N} \frac{|L_{F,i} - \overline{L}_F|}{\overline{L}_F} \quad (3)$$

2.3.2. Wet weight determination and chlorophyll a quantification

The determination of cyanobacterial biofilms wet weight and chlorophyll *a* content was performed as reported in Romeu et al. (2019). In order to determine the wet weight, coupons were detached from the wells and weighed. Biofilm wet weight was obtained as the difference from the initial coupon weight (determined prior to inoculation). Afterwards, cyanobacterial cells were detached from the coupons by immersing each coupon in 2 ml of 8.5 g l^{-1} sodium chloride solution and vortexing. The suspensions were incubated for 24 h at 4 °C in the dark and chlorophyll *a* determination was performed as previously described through Eq. (1).

2.3.3. Crystal violet assay

Additional coupons, representative of all conditions, were transferred to sterile 24-well plates at each sampling day. Crystal violet assay was adapted from a previously described protocol (Moreira et al., 2017). Briefly, to fix the cyanobacterial biofilms, 1 ml of 100% (v/v) ethanol was added to each well for 15 min. Afterwards, culture plates were allowed to air dry at room temperature. The fixed biofilms were stained with 1 ml of 1% (v/v) crystal violet solution (Merck KGaA, Germany) for 5 min and to solubilize the crystal violet (CV), 1 ml of 33% (v/v) acetic acid (VWR, Portugal) was added to each well. Then, 200 μL of this solution was transferred to sterile 96-well plates, and the optical density was measured at 570 nm in a plate reader (SpectroStar Nano, BMG LABTECH).

2.3.4. Statistical analysis of biofilm development

A total of six replicates (two biological assays with three technical replicates each) were analysed. Data analysis was performed using the statistical program GraphPad Prism® for Windows, version 6.01 (GraphPad Software, Inc., San Diego, CA, USA) and results were compared using unpaired t-tests with a confidence level of 95% (**; $P < 0.05$) and 90% (*; $P < 0.1$).

2.4. Proteomics analysis

2.4.1. Protein extraction and sample preparation

At the last sampling time (49 days), biofilm samples of unidentified filamentous cyanobacterium LEGE 06007 strain from each condition were recovered for proteomic analysis and processed as previously described (Romeu et al., 2020) with some modifications. Briefly, cyanobacterial biofilms were detached from the surface by immersing each coupon in 2 ml of 8.5 g l^{-1} sodium chloride solution and vortexing. To maximise the biomass yield, suspensions obtained from four coupons of the same condition were pooled. The samples were centrifuged at 3202 g for 10 min at room temperature and the pellets of biomass originating from 24 biofilm samples comprising six independent-replicates from four different growing conditions were kept at −20 °C for further processing. Following previously described protocols (Campos et al., 2016), the amount of sample was calculated, and an appropriate volume of SDT buffer (0.5 g FW/ml SDT) + Protease inhibitors (PIs, Roche, 11697498001, Basel, Switzerland) was added to the samples. These were sonicated 10 × 3 s and 23 kHz–105 μm (amplitude) and incubated for 4 h at room temperature. Then, samples were heated for 3 min at 95 °C and subsequently centrifuged at 16,000 g for 20 min. Finally, the supernatant was collected, and total protein concentration was measured indirectly

by optical density (OD) at 280 nm using a DeNovix DS-11 Spectrophotometer (DeNovix Technologies, Wilmington, Delaware, USA). Samples containing the extracted protein were stored for 24 h at −20 °C.

The extracted proteins were processed using two distinct protocols based on FASP protocol described by Wiśniewski et al. (2009) and the SP3 (Hughes et al., 2019) technology.

2.4.1.1. FASP. Similar to previous works, the samples containing the extracted proteins stored at −20 °C were defrosted in ice for further processing using the FASP protocol as previously described (Almeida et al., 2020; Martins et al., 2020; Matos et al., 2020; Romeu et al., 2020). This approach comprised the alkylation with iodoacetamide and digestion of 40 μg of the extracted proteins with trypsin (recombinant, proteomics grade, Roche, Basel, Switzerland) at an enzyme to protein ratio of 1:100 (w/w) for 16 h at 37 °C using centrifugal filter units with nominal molecular weight limit (NMWL) of 30 kDa (MRCPRT030, Millipore, Billerica, MA, USA). Through centrifugal filtration, peptides were recovered and acidified with Trifluoracetic acid (TFA: 10% v/v). Samples were desalted and concentrated by reversed-phase extractions (C18 Tips, 100 μL, Thermo Scientific, Thermo Fisher Scientific, Wilmington, DE, USA) with acetonitrile (CAN: 50% v/v) and TFA (0.1% v/v) for peptide elution. Before LC-MS/MS analysis, samples were dried in a Concentrator Plus vacuum rotator (Eppendorf, Hamburg, Germany) and resuspended in 25 μL formic acid (FA: 0.1% v/v). The final concentration was determined with 2 μL of digested peptides, measured indirectly by optical density (OD) at 280 nm using a DeNovix DS-11 Spectrophotometer (DeNovix Technologies, Wilmington, Delaware, USA).

2.4.1.2. SP3. Prior to digestion, 100 μg of extracted proteins in approximately 5 μL were reduced in 45 μL SDT in new 1.5 mL Eppendorf tubes. Then, alkylation of samples was performed with 10 μL of 0.1 M iodoacetamide (AppliChem) in 8 M Urea, 0.1 M Tris/HCl pH 8.5 for 30 min in the dark at room temperature.

Digestion followed Hughes et al. (2019) SP3 for proteomics experiments with some modifications. New magnetized beads (Sera Mag SP3 beads, CAT#45152105050250 and CAT#65152105050250, GE Healthcare) were initially washed and reconstituted in water (HPLC grade, VWR) at a final concentration of 10 μg/μL (from an initial stock concentration of 50 mg/mL), using a magnetic rack (MagnaRack, Invitrogen) for 1 min, and the protein digestion was conducted according to specifications of the manufacturer. Then, after removing the supernatant, 100 μL ammonium bicarbonate (Fluka) 0.05 M was added to the tubes and incubated for 5 min at 1000 rpm. After bead spin and magnetizing, the supernatant containing the tryptic peptides was transferred to clean 1.5 mL Eppendorf tubes. The peptide concentration was estimated using the DeNovix (A280 application). Acidification was performed by adding 20 μL of formic acid 5% v/v (Optima LC/MS grade, Fisher Chemical) to the samples. Afterwards, tryptic peptides were dried in a Concentrator Plus vacuum rotator (Eppendorf, Hamburg, Germany) and resuspended in 25 μL formic acid (FA: 0.1% v/v). The final concentration was determined with 2 μL of digested peptides, measured indirectly by optical density (OD) at 280 nm using a DeNovix DS-11 Spectrophotometer (DeNovix Technologies, Wilmington, Delaware, USA). A detailed description of the SP3 protocol can be found in Appendix A.

2.4.2. LC-MS/MS analysis

Considering that both sample preparation methods are complementary, tryptic peptides from both methods were mixed in the same tube to a final concentration of 0.1 μg and 0.5 μg from FASP and SP3, respectively. Then, protein digests from both protocols were analysed in the same run with a nano LC-MS/MS, composed by an Ultimate 3000 liquid chromatography system coupled to a Q-Exactive Hybrid Quadrupole – Orbitrap mass spectrometer (Thermo Scientific, Bremen, Germany), as previously described (Osório et al., 2021). Separation was performed in a 15 cm by 75 μm inner diameter EASY-Spray column (ES800, PepMap RSLC, C18, 3 μm, Thermo Scientific, Bremen, Germany) at 300 nL/min using a gradient generated by mixing A: 0.1% FA and B: 80% ACN, in the following quantities: 5 min (2.5% B to 10% B), 60 min (10% B to 35% B), 5 min (35% B to 99% B) and 5 min (hold 99% B). Subsequently, the column was equilibrated with 2.5% B for 12 min. Data acquisition was controlled by Xcalibur 4.0 and Tune 2.8 software (Thermo Scientific, Bremen, Germany). The specific LC-MS parameters were full scan settings: 70 k resolution (m/z 200), AGC target 3e6, maximum injection time 50 ms dd settings: minimum AGC target 8e3, intensity threshold 7.3e4, charge exclusion: unassigned, 1, 8, >8, peptide match preferred, exclude isotopes on, dynamic exclusion 20s. MS2 settings: microscans 1, resolution 35 k (m/z 200), AGC target 2e5, maximum injection time 110 ms, isolation window 2.0 m/z, isolation offset 0.0 m/z, spectrum data type profile.

2.4.3. Protein identification

The raw data was analysed and processed using the Proteome Discoverer 2.2.0.388 software (Thermo Scientific) and searched against the UniProt database for Cyanobacteria taxonomic selection (2018_07 release). The Sequest HT search engine was used for protein identification. The ion mass tolerance was 10 ppm for precursor ions and 0.02 Da for-fragment ions. Maximum allowed missing cleavage sites was set to 2. Cysteine carbamidomethylation was defined as a constant modification. Methionine oxidation and protein N-terminus acetylation were defined as variable modifications. Peptide confidence was set to high. The processing node Percolator was enabled with the following settings: maximum delta Cn 0.05; decoy database search target false discovery rates (FDR) 1%, validation was based on q-value. Protein label-free quantitation was performed with the Minora feature detector node at the processing step. Precursor ion quantification was performed at the processing step with the following parameters: unique plus razor peptides were considered for quantification and precursor abundance was based on intensity.

2.4.4. Differential protein expression and enrichment

Statistical analyses applied to the proteomic data were performed using R software version 4.0.0. (Dessau and Pipper, 2008). The Differentially Expressed Proteins (DEPs) and/or gene enrichment were assessed using the "DEP" R package (Zhang et al., 2018), based on the *limma* algorithm (Ritchie et al., 2015). Missing values were filtered according to the fraction of protein found in each paired comparison with a cut-off of 0.33%, considering the possibility of having a minimum of 4 out of 6 replicates of at least one condition. Imputation of missing values was performed considering a non-random distribution (MNAR) using "MinProb" as an imputation function. Significant differences between conditions for each condition were paired tested by protein-wise linear models and empirical Bayes statistics. Finally, adjusted P-value (alpha = 0.05), and the $\log_2$ fold change (lfc = $\log_2(1.5)$, $\log_2$ fold change >0.6) were used as a filter threshold to classify them as DEPs or enriched genes. For comparison purposes, the distribution of DEPs among conditions was analysed by Venn diagrams using an online free tool, available at the webserver of the Bioinformatics and Evolutionary Genomics Center (BEG/Van de Peer Lab site), Ghent University, Belgium, http://bioinformatics.psb.ugent.be/webtools/Venn/.

2.4.5. Functional annotation

Functional classification (gene ontology) was carried out using the OmicsBox software version 1.4.11 (https://www.biobam.com/omicsbox/). Protein signatures were also obtained from the InterPro member databases (*e.g.* Pfam, PROSITE, PRINTS, ProDom, SMART, TIGRFAMs, PIRSF, SUPERFAMILY, Gene3D, and PANTHER) using the InterProScan software (Mitchell et al., 2019) integrated into the OmicsBox tool. All annotation and the corresponding gene ontology (GO) terms were then

transferred to the sequences and eventually merged with existing GO terms resulting from blast search. Additional functional analyses to determine over/underexpressed pathways were performed to the categorical GO terms corresponding to DEPs, using the hypergeometric distribution significance test (Fisher's exact test, $P < 0.05$).

3. Results and discussion

3.1. Biofilm development analysis

Cyanobacterial biofilm development was assessed for 49 days, and the wet weight, chlorophyll *a* content, total biomass and thickness evolution is shown in Fig. 1. Biofilm biomass was higher at the lowest shear rate for both surfaces, as it is particularly noticeable in the biofilm thickness obtained on glass (Fig. 1G). Previous studies performed with different filamentous cyanobacterial strains have shown that despite the tenfold difference in average shear rate, cyanobacterial biofilm behavior was similar in both hydrodynamic conditions for the first weeks of biofilm development (Romeu et al., 2019, 2020). In the present study, differences in biofilm development at different shear conditions were noticed in the early stages, but major differences were also found in the maturation phase of biofilm development. It is possible that sloughing and erosion events related to the shear rate also assume particular significance at later stages of biofilm development. Similar results were also obtained with coccoid cyanobacteria, *Synechocystis salina* and *Cyanobium* sp. strains, when glass and a polymeric epoxy coating were used (Faria et al., 2020a). The major differences between the two hydrodynamic conditions were observed from data obtained from thickness quantification (Fig. 1G and H) but also from biofilm wet weight (Fig. 1A and B). Biofilm mass obtained on glass under lower shear conditions (4 s^{-1}) was on average 71.5% higher when compared to the values obtained at a higher shear rate (40 s^{-1}; Fig. 1A). On perspex, biofilm wet weight at 4 s^{-1} was on average 53.9% higher (Fig. 1B). Whereas chlorophyll *a* content at 4 s^{-1} on glass and perspex was on

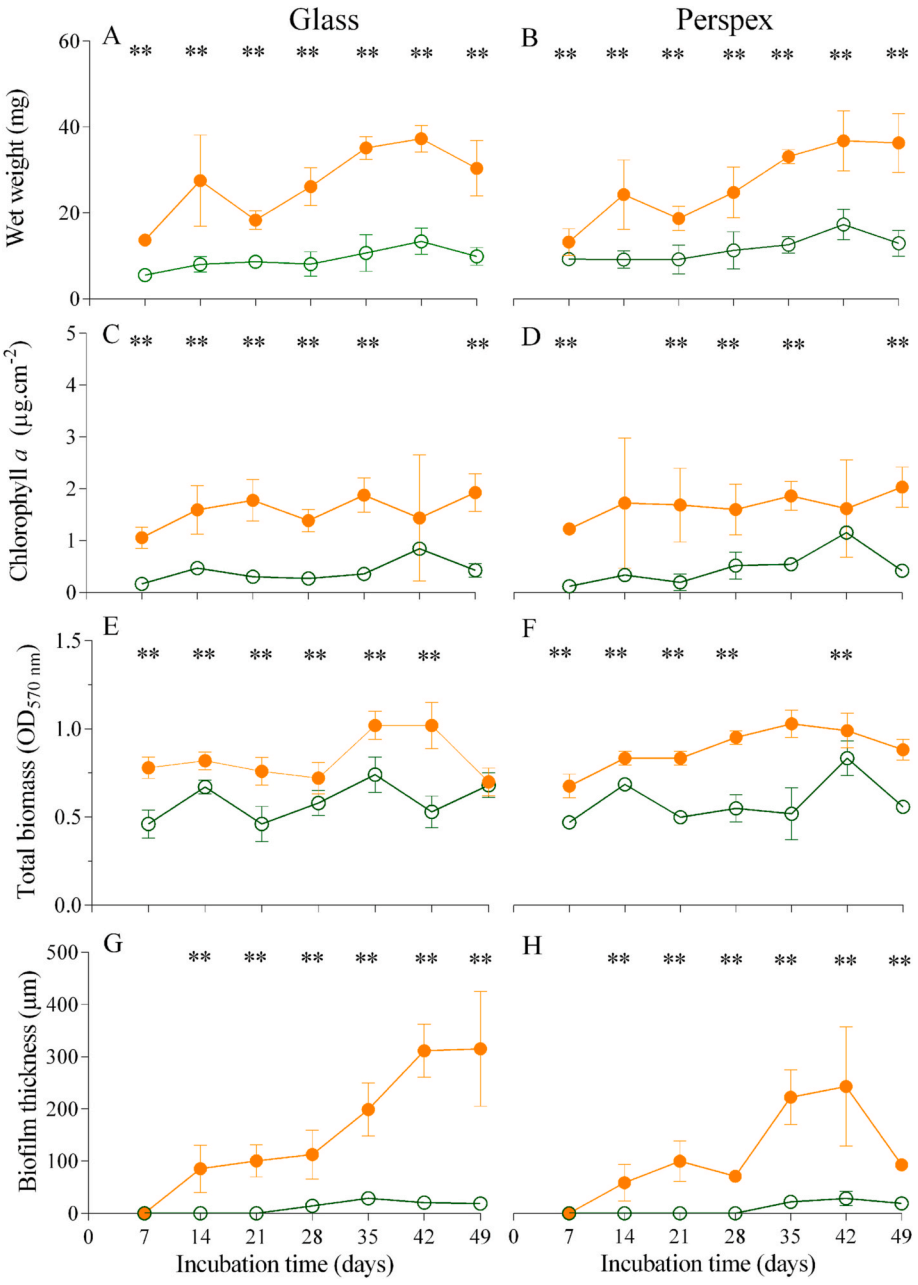

Fig. 1. Evaluation of unidentified filamentous cyanobacterium LEGE 06007 biofilm development. The parameters analysed refer to wet weight (A, B), chlorophyll *a* quantification (C, D), total biomass quantification by CV assay (E, F) and biofilm thickness (G, H). Biofilms were formed in glass (A, C, E, G) or perspex (B, D, F, H), at two average shear rates, 4 s^{-1} (closed circles, orange) and 40 s^{-1} (open circles, green) for 49 days. Standard deviations from two biological assays with three replicates each are represented. Symbol ** indicate statistically different values for $P < 0.05$ at each incubation time. (For interpretation of the references to colour in this figure legend, the reader is referred to the Web version of this article.)

average 75% higher (Fig. 1C and D) than at higher shear conditions. As previously reported (Chorus and Cavalieri, 2000; Romeu et al., 2019, 2020), chlorophyll *a* content monitorisation demonstrated to be a useful tool to follow cyanobacterial biofilm growth since a correlation between chlorophyll *a* production and biofilm wet weight was observed (Appendix B). Due to the complexity of filamentous cyanobacteria, there is a need to develop novel methodologies to study these organisms. To evaluate if the crystal violet assay (CV) can be a suitable approach for cyanobacterial biofilms analysis, quantification of total biomass was performed by CV. On glass, the total biomass quantified by this method was on average 28.1% higher at lower shear when compared to the values obtained at a higher shear rate (40 s^{-1}; Fig. 1E), whereas on perspex the average value obtained was about 33.2% higher at 4 s^{-1} (Fig. 1F). Data obtained from this parameter corroborates observations from additional parameters, since higher biofilm biomass was obtained at the lowest shear rate for both surfaces. A correlation between data obtained from total biomass quantification by CV and biofilm thickness and from wet weight was observed (Appendix C and D, respectively). Therefore, based on the results obtained for this strain, the quantification of total biomass from CV demonstrated to be useful tool to follow cyanobacterial biofilm growth.

Similar values of wet weight, chlorophyll *a* content, total biomass quantification and biofilm thickness were obtained for biofilms developed on different surfaces at the same hydrodynamic conditions (Appendix E), showing that the effect of surface properties was less important than the hydrodynamic effect on cyanobacterial biofilm development in a macroscopic biofilm evaluation. Despite the different hydrophobicity of glass and perspex (Romeu et al., 2019), these findings had already been shown for other coccoid (Faria et al., 2020a) and filamentous cyanobacterial strains (Romeu et al., 2019, 2020).

OCT analysis was used to analyse biofilm roughness and structure at different conditions. Biofilm roughness was only evaluated in the maturation phase of biofilm development, in which differences in biofilm thickness were more evident (from day 35). The analysis revealed that biofilms formed under the lower shear rate showed lower roughness coefficient values than those formed at higher shear on both surfaces (Appendix F). Once again, the values obtained from biofilms developed under the same hydrodynamic condition at different surfaces were very similar. Fig. 2 shows representative 2D cross-sectional images obtained from OCT at the end of the experiment (49 days). These figures highlight the importance of the hydrodynamic effect when compared to the surface effect. Previous studies showed that cyanobacterial biofilms developed under higher shear rates present a more compact structure (Romeu et al., 2019, 2020), which probably increases biofilm cohesion (Teodósio et al., 2011). In this study, the low biofilm biomass obtained under a higher shear rate (40 s^{-1}) on both surfaces (Fig. 2 B, D) did not enable a comprehensive interpretation of biofilm structure and compaction.

Excessive shear stress can cause increased cell mortality, decreased growth rate and cell viability, or even cell lysis. Different organisms have different tolerances for the damage caused by hydrodynamic forces (Sobczuk et al., 2006). Among photosynthetic organisms, green algae have the greatest tolerance to shear stress, followed by cyanobacteria, red algae and diatoms, with dinoflagellates comprising the most shear-sensitive species (Wang and Lan, 2018). In these organisms, the shear-sensitivity is determined primarily by cell wall strength, cell morphology and the presence of flagella. Cyanobacterial cell walls are mainly composed by peptidoglycan, they comprise three to four layers and range from 10 to 20 nm in thickness and an envelope may also surround the cell to form a sheath (Stanier and Cohen-Bazire, 1977). On biofilms, as cells are embedded in a matrix mainly composed by extracellular polymeric substances (EPS), the interaction between EPS components promotes biofilm cohesion, with stronger EPS interactions preventing biofilm mechanical failure (Cense et al., 2006). Moreover, it has been recognized that biofilms are viscoelastic materials (Gloag et al., 2020). Viscoelasticity allows biofilm survival, promoting the formation of stronger biofilms when exposed to higher shear forces. Therefore, viscoelasticity emerged as a general survival adaptation for biofilms in the surrounding environment, such as shear stresses. Several studies showed that viscoelasticity is an emergent behavior of bacteria when they form biofilms, and that these properties are largely governed by EPS (Peterson et al., 2013). In our study, if some cells rupture, the impact of organic matter release from the cells may not have a significant impact on biofilm development since the surrounding environment is constantly renewed.

3.2. Proteomic analysis

This work revealed for the first time the differential proteome expression of cyanobacterial biofilm cells developed in different conditions. Overall, 546 proteins were identified through the shotgun proteomics analysis from 24 biofilm samples of four different conditions (Appendix G). Herein, the total number of protein identified was relatively higher than a previous qualitative proteomic study performed on two different cyanobacterial strains at the same biofilm conditions (Romeu et al., 2020). Similar to the aforementioned study, most of the proteins identified in this work corresponded to intracellular proteins since the surrounding environment, supernatant and exudate were not analysed. However, excreted proteins may have also been identified since they may have been retained in the biofilm matrix.

3.2.1. Enrichment and distribution of DEPs among conditions

The quantitative proteomic analysis was performed with the "DEP" R package (Zhang et al., 2018), revealing a total of 41 DEPs (Fig. 3, Table 1). Some of these DEPs were also previously identified in the qualitative approach from different cyanobacterial strains (Romeu et al., 2020). Among these proteins, ribosomal proteins were found, and others involved in photosynthesis and respiration, which are essential in primary metabolic functions, as well as proteins associated with phycobilisomes and elongation factors. Although a macroscopic evaluation of biofilm revealed a greater difference between the two hydrodynamic conditions, the proteomic analysis showed a higher difference in protein expression between the biofilms formed on glass and perspex at 4 s^{-1}, followed by the biofilms formed on glass at 4 s^{-1} and 40 s^{-1}, which demonstrated the importance of studies addressing different approaches. Indeed, among the four comparisons performed, most of the proteomic variations corresponded to the paired-comparison between samples from glass *vs* perspex at 4 s^{-1} (Fig. 3A). In this comparison, 34

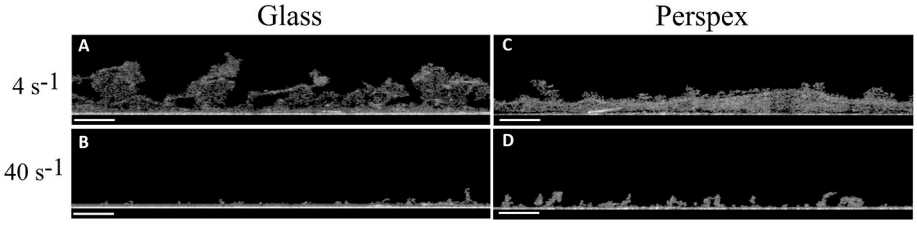

Fig. 2. 2D cross-sectional OCT images of unidentified filamentous cyanobacterium LEGE 06007 biofilms formed after 49 days on glass and perspex at two different shear rates, 4 s^{-1} (A, C) and 40 s^{-1} (B, D). Scale bar = 200 μm.

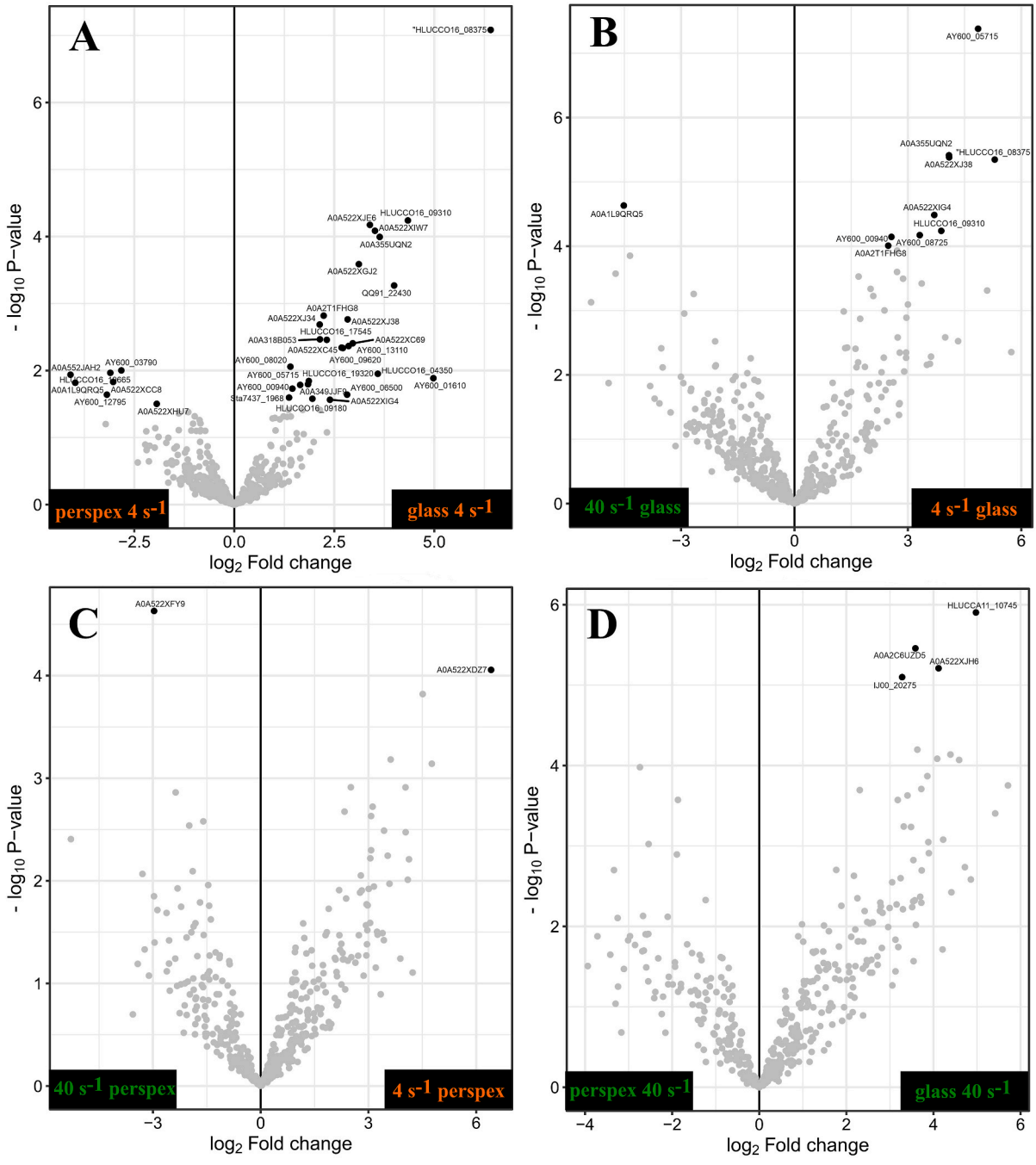

Fig. 3. Volcano plot of the differentially expressed proteins (DEPs) among the 4 biofilm conditions studied. Black points represent the DEPs showing the corresponding gene symbol, or the protein accession number when lacking the corresponding gene annotation. The axis depicts the *P* values ($-\log_{10}$) plotted against the fold changes ($\log_2$) between each paired-comparison. A) glass *vs* perspex at 4 s^{-1} (down and up-regulated proteins on glass at 4 s^{-1} when compared with perspex at 4 s^{-1}); B) 4 s^{-1} *vs* 40 s^{-1} on glass (down and up-regulated proteins at 4 s^{-1} on glass when compared with 40 s^{-1} on glass); C) 4 s^{-1} *vs* 40 s^{-1} on perspex (down and up-regulated proteins at 4 s^{-1} on perspex when compared with 40 s^{-1} on perspex); D) glass *vs* perspex at 40 s^{-1} (down and up-regulated proteins on glass at 40 s^{-1} when compared with perspex at 40 s^{-1}).

DEPs were found, where 27 DEPs were up-regulated and seven down-regulated in the glass surface relatively to perspex (Fig. 3A). 10 DEPs were identified in the comparison between at 4 s^{-1} *vs* 40 s^{-1} on glass (Fig. 3B), whereas two DEPs were found between samples from biofilms developed at 4 s^{-1} *vs* 40 s^{-1} on perspex (Fig. 3C). Finally, four up-regulated DEPs were revealed in the glass surface relatively to perspex in comparing between biofilms developed on glass vs perspex at 40 s^{-1}, (Fig. 3D).

3.2.2. Linking DEPs to the functional categories involved

Around 39.6% of the DEPs were related to metabolic processes and 11% with transport (Appendix H). Additionally, 4.9% and 3.3% were associated with the regulation of biological processes and response to a stimulus, respectively. Among the 34 DEPs identified on the glass surface relatively to perspex (Fig. 3A), nine of them overlapped with results from biofilm cells formed on glass at 4 s^{-1} vs 40 s^{-1} (Figs. 3B and 4). It is noteworthy that among these nine DEPs, a protein related to allophycocyanin was down-regulated in both comparisons, which suggests that

Table 1
List of the 41 DEPs and their corresponding accession number (Protein IDs), gene names, description and the log_2 fold-changes obtained from each comparison.

UniProt accession number	Gene Names	Description	glass *vs* perspex at 4 s^{-1}	4 s^{-1} *vs* 40 s^{-1} on glass	4 s^{-1} *vs* 40 s^{-1} on perspex	glass *vs* perspex at 40 s^{-1}
A0A0P8BXS9	HLUCCO16_08375	Uncharacterized protein (Fragment)	6.41	5.30		
A0A1L9QRQ5		Allophycocyanin	−3.98	−4.51		
A0A2T1FHG8		Elongation factor Tu	2.23	2.48		
A0A318B053		Aldehyde dehydrogenase	2.14			
A0A349JJF9		SLH domain-containing protein (Fragment)	1.84			
A0A355UQN2		50 S ribosomal protein L5	3.64	4.09		
A0A522XC45		Photosystem II CP43 reaction center protein	2.68			
A0A522XC69		Alpha/beta hydrolase	2.96			
A0A522XCC8		Isoleucine–tRNA ligase (Fragment)	−3.03			
A0A522XGJ2		SLH domain-containing protein	3.11			
A0A522XHU7		60 kDa chaperonin	−1.94			
A0A522XIG4		30 S ribosomal protein S8	2.39	3.70		
A0A522XIW7		O-acetylhomoserine aminocarboxypropyltransferase/cysteine synthase	3.52			
A0A522XJ34		50 S ribosomal protein L1	2.13			
A0A522XJ38		Phycobilisome rod-core linker polypeptide CpcG	2.83	4.09		
A0A522XJE6		Gfo/Idh/MocA family oxidoreductase	3.39			
A0A552JAH2		Chaperone protein DnaK	−4.10			
A0A168VPC8	AY600_00940	Uncharacterized protein	1.45	2.56		
A0A168UQZ4	AY600_01610	Cytochrome *c*-550	4.98			
A0A168SDR0	AY600_03790	Ferredoxin–NADP reductase	−2.83			
A0A168SSA6	AY600_05715	Cytochrome *c*6	1.65	4.86		
A0A168VLH9	AY600_06500	Uncharacterized protein	2.82			
A0A168WPD9	AY600_08020	Uncharacterized protein	1.40			
A0A168VRY4	AY600_09620	Beta-propeller domain-containing protein, methanol dehydrogenase	2.71			
A0A168UP82	AY600_12795	Elongation factor P	−3.19			
A0A168VMU3	AY600_13110	Ferredoxin	2.86			
A0A0P7Z9L3	HLUCCO16_04350	Photosystem I reaction center subunit XI	3.59			
A0A0P8DQC9	HLUCCO16_09180	Uncharacterized protein	1.95			
A0A0N8KPF0	HLUCCO16_09310	ATP synthase subunit delta	4.34	3.88		
A0A0P7ZV78	HLUCCO16_17545	OMF family outer membrane protein	2.31			
A0A0P8BGT0	HLUCCO16_19320	Phosphomannomutase	1.86			
A0A0P8BV27	HLUCCO16_19665	Uncharacterized protein	−3.10			
A0A0C1UQ05	QQ91_22430	Aconitate hydratase	4,00			
K9XV32	Sta7437_1968	Polyribonucleotide nucleotidyltransferase	1.37			
A0A168SH97	AY600_08725	Uncharacterized protein		3.31		
A0A522XDZ7		Superoxide dismutase			6.42	
A0A522XFY9		Uncharacterized protein			−2.97	
A0A2C6UZD5		Aldehyde dehydrogenase (Fragment)				3.59
A0A522XJH6		DUF2862 domain-containing protein				4.12
A0A0P8BNN3	HLUCCA11_10745	Phycocyanin, beta subunit				4.98
A0A0T7BVN2	IJ00_20275	Elongation factor Tu				3.28

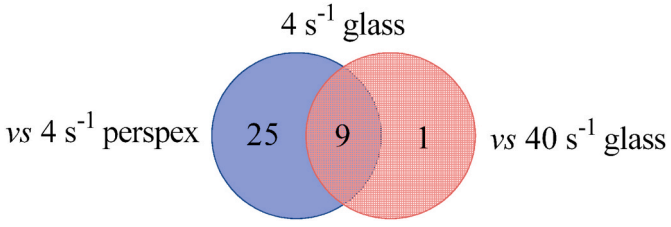

Fig. 4. Venn diagram displaying the unique and shared DEPs found between 4 s^{-1} glass *vs* 4 s^{-1} perpex and 4 s^{-1} glass *vs* 40 s^{-1} glass.

compared to perspex at 40 s^{-1}, the expression of this phycobiliprotein was decreased on glass (Fig. 3A) and at 4 s^{-1}, respectively (Fig. 3B, Table 1).

The same 8 up-regulated proteins were identified when comparing biofilms formed on glass and perspex at 4 s^{-1} (Fig. 3A) and when comparing biofilms formed on glass at both shear rates (Fig. 3B, Table 1). These proteins are mainly involved in metabolic process, photosynthetic activity, binding and transport, similarly to the unique 19 up-regulated sequences found in the biofilms developed on glass at 4 s^{-1} in comparison to perspex (Fig. 5). Among the eight shared proteins, a protein related to elongation factor Tu was identified (A0A2T1FHG8, Fig. 3A and B, Table 1). Indeed, elongation factors have already been described as virulence factors and associated with filament formation (López-Ochoa et al., 2017) and biofilm formation (Qayyum et al., 2016) in different organisms (Harvey et al., 2019). However, from the data obtained in the present study, it is possible to consider that this may not be the major factor for increased biofilm development. In fact, the up-regulation of an additional elongation factor Tu was also observed on biofilm cells developed at 40 s^{-1} in glass compared to perspex (A0A0T7BVN2; Table 1), and no considerable biofilm increase was observed in that case (Appendix E, Figure E.1 B, D, F, H). Moreover, an elongation factor P (AY600_12795) was down-regulated on glass when compared to biofilms formed on perspex at 4 s^{-1} (Fig. 3A, Table 1). Therefore, additional pathways and/or factors must have contributed to cyanobacterial biofilm development in these conditions. Additional up-regulated proteins shared between biofilms formed on glass and perspex at 4 s^{-1} (Fig. 3A) and biofilms developed at 4 s^{-1} and 40 s^{-1} on glass (Fig. 3B) include ribosomal proteins, proteins related to phycobilisome rod-core linker polypeptide CpcG, cytochrome *c*6, ATP synthase and two uncharacterized proteins (Table 1). It is noteworthy that both ribosomal proteins and those related to photosynthesis, as well as phycobilisome rod-core linker polypeptide CpcG have already been found in a previous qualitative proteomic study performed on biofilm cells from two different cyanobacterial species (Romeu et al., 2020). Since the same surfaces and hydrodynamic conditions were used in both studies, this suggests the relevance of this set of proteins in the cyanobacterial

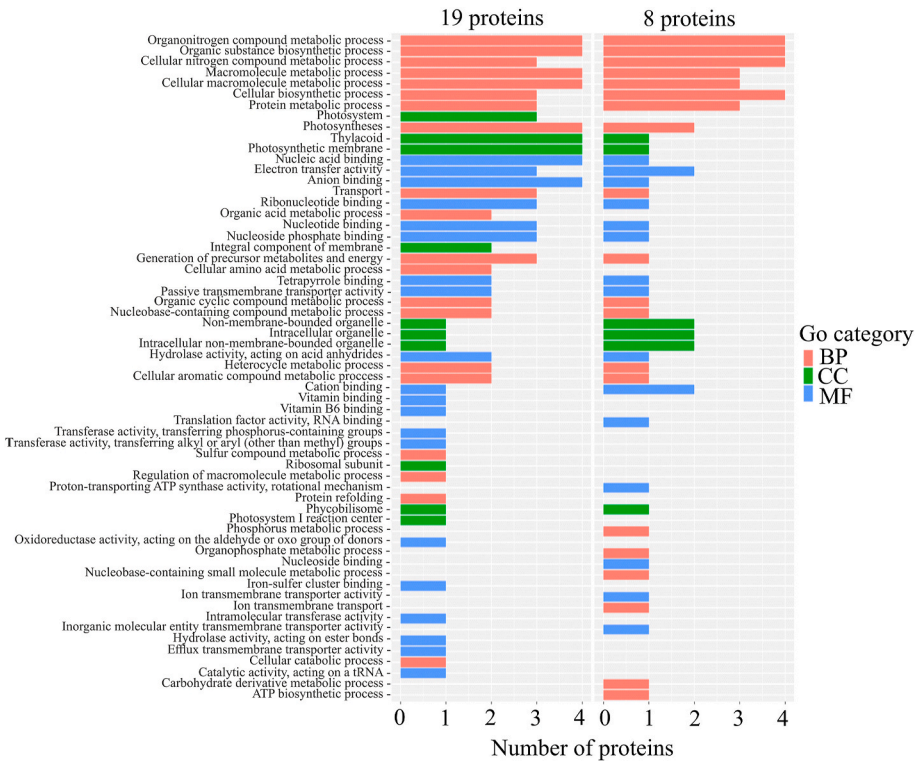

Fig. 5. Functional annotation of the three major GO Categories: Biological Process (BP), Molecular Function (MF) and Cellular Components (CC) according to the GO Distribution by Level (4). The figure shows the number of sequences (number of proteins) in a descendent manner matching GO-terms of the unique up-regulated DEPs (19 proteins) and the eight shared DEPs (8 proteins), overlapped between the comparison glass *vs* perspex at 4 s^{-1} and 4 s^{-1} *vs* 40 s^{-1} on glass. More details about GO annotation can be found in the Appendix I.

biofilm development in these conditions.

Among the two uncharacterized proteins shared between these two paired-comparison, proteins involved in the electron transport pathway of photosynthesis activity (A0A0P8BXS9) and related with calcium ion binding (A0A168VPC8) were identified. In addition, the unique protein not shared between glass *vs* perspex at 4 s^{-1} and 4 s^{-1} *vs* 40 s^{-1} on glass conditions was also an uncharacterized protein related to calcium ion binding (A0A168SH97, Fig. 4, Table 1), suggesting that calcium may play an important role in these cyanobacterial biofilms. Moreover, these two uncharacterized proteins related to calcium ion binding are disordered proteins. Although disordered proteins do not have unique structures, they possess biological functions. It is expected that disordered proteins possess some advantages over ordered proteins due their exceptional spatio-temporal heterogeneity and high conformational flexibility (Uversky, 2019). Indeed, they are more likely to maintain stability under extreme conditions due to the lack of structural conservation (Liu and Huang, 2014). In a real scenario, these proteins can perform their functions in complex environments, which can be affected by various factors such as hydrodynamic conditions or surface properties. Several proteins with disordered domains were identified in the cement-multicomplex adhesive-system from goose barnacles, applying a similar proteogenomic approach (Domínguez-Pérez et al., 2020, 2021). Moreover, additional studies described surface-coupling proteins as structurally disordered, which confers them elasticity (Cheng et al., 2010; Wang et al., 2018a).

Between the unique 19 up-regulated sequences found in the biofilms developed on glass at 4 s^{-1} when compared to perspex (Figs. 3A and 5, Table 1), uncharacterized proteins were also differentially expressed including one disordered protein (A0A168VLH9). In addition, proteins like a beta-propeller domain-containing protein, a methanol dehydrogenase (AY600_09620), the chaperone protein DnaK (A0A552JAH2), SLH domain-containing proteins (A0A349JJF9 and A0A522XGJ2) and OMF family outer membrane protein (HLUCCO16_17545) were also identified as DEPs. Although secreted beta-propeller proteins are largely unexplored in bacteria and even more in cyanobacteria, some studies suggest that they may be involved in the maintenance of the cell envelope, secretion, adhesion, and host immune responses (Fu et al., 2018; Kim et al., 2018). A study on *Vibrio cholerae* biofilms showed that the beta-propeller domains might form interactions with proteins or other substrates (including polysaccharides) within the biofilm matrix (Kaus et al., 2019). In a study on *Acinetobacter baumannii* cells it was observed that the expression of a chaperone-usher secretion system is required for pili formation and the concomitant attachment to plastic surfaces and biofilm formation (Tomaras et al., 2003). DnaJ2 and DnaK2 together behave as an RNA chaperone shielding the psbAII transcript from RNaseE-intervened degradation, in this way helping to prevent the inhibition of photosynthesis under conditions of stress (Ehrnsperger et al., 1997). Although cyanobacteria have many dnaK genes in their genome (Haslbeck et al., 2005), there is no knowledge regarding their relation to biofilm development. S-layer homology (SLH) domains are cell wall-targeting modules employed by various Gram-positive and -negative bacteria to display extracellular proteins such as enzymes and outer membrane proteins on the bacterial cell surface (Engelhardt and Peters, 1998). A study performed by Janesch et al. 2013), demonstrated the involvement of the SLH domain-containing protein SlhA in swarming and biofilm formation of *Paenibacillus alvei* (Janesch et al., 2013). Outer membrane proteins and outer membrane vesicles (OMV) have been relevant in biofilm studies. It was demonstrated that *Helicobacter pylori* TK1402 exhibited a strong ability for biofilm formation, and its OMVs play an important role in the formation of their extracellular matrix (Yonezawa et al., 2011). A proteomic study of *Burkholderia multivorans* C1576 revealed that OMVs production is the most important source of proteins for the biofilm matrix (Terán et al., 2020). OMVs are highly enriched in outer membrane proteins and siderophores. Of note, some of the identified proteins were proteins involved in reactive oxygen species (ROS) scavenging. Therefore, proteins responsible for detoxification of ROS are also a relevant fraction of both matrix- and OMVs-associated proteins. Accordingly, the data obtained in this study showed the possible role of a beta-propeller domain-containing protein, chaperone DnaK, SLH domain-containing proteins and an OMF family outer membrane protein on biofilm developed on glass at 4 s^{-1} in comparison to perspex for this cyanobacterial strain (Figs. 3A and 5,

Table 1).

Additionally, biofilm development on perspex at 4 s^{-1} was higher than at 40 s^{-1} (Fig. 1B, D, F). The proteomic analysis only revealed the underexpression of an uncharacterized protein (A0A522XFY9) and overexpression of an enzyme, superoxide dismutase (SOD) at 4 s^{-1} (A0A522XDZ7, Fig. 3C, Table 1) when compared with biofilm formed at 40 s^{-1}. Similar to previous uncharacterized proteins, the down-regulated protein identified in this paired comparison presented a disordered domain. SOD are ubiquitous enzymes that scavenge superoxide radicals to peroxide and molecular oxygen through alternate oxidation and reduction of their metal ions. Since cyanobacteria produce ROS that can damage cellular components leading to cell death, the co-evolution of an antioxidant system was necessary for their survival and SOD is the initial enzyme evolved to alleviate this toxic effect (Priya et al., 2007). Several SOD genes were found on cyanobacteria strains (Kaneko et al., 1996; Shirkey et al., 2000; Zhao et al., 2007), even on filamentous strains (Campbell and Laudenbach, 1995; Priya et al., 2007). Besides their role in oxidative stress and resistance, the relevance of SOD has already been reported in several studies from other bacteria than cyanobacteria on adhesion, biofilm formation and invasion of epithelial cells (Bink et al., 2011; Najmuldeen et al., 2019; Suo et al., 2012; Trémoulet et al., 2002; Wang et al., 2018b). Therefore, the higher biofilm development observed on perspex at 4 s^{-1} can also be related to the up-regulation of this enzyme in this filamentous cyanobacterial strain.

Moreover, with a higher biofilm development at 4 s^{-1}, the production of ROS may have increased along with respiration and photosynthesis, which may have prompted an increased activity of this enzyme to prevent damage caused by oxidative stress. A study on *Klebsiella pneumoniae* also shows the role of SOD in biofilm architecture and cell morphology (Najmuldeen et al., 2019). Although the detailed mechanisms of alterations in biofilm architecture are unclear, it could be speculated that *Klebsiella pneumoniae* biofilm architecture is significantly influenced by oxygen and by the activity of SOD. Therefore, alteration in biofilm architecture might occur in response to redox balance, which is essential for cellular function and survival. In the present study, a different structure was also observed for biofilms developed on perspex at 4 s^{-1} and 40 s^{-1} (Fig. 3C and D). Once again, SOD can present an active role in the biofilm architecture of this cyanobacterial strain between biofilms developed on perspex at 4 s^{-1} and 40 s^{-1}. The proteomic changes of SOD on all replicates from each condition throughout the experiment can be found in Appendix J.

Finally, the total of 27 up-regulated DEPs found on biofilm cells from glass at 4 s^{-1} compared to perspex, shows a different enrichment pattern than the seven down-regulated DEPs at the same condition when compared to the ones encoded in the whole proteome (Fig. 6). In the 27 up-regulated DEPs, the GO terms "electron transfer activity" and "electron transport chain", processes related to electron chain and actively involved in photosynthesis, were found as enriched categories (Fig. 6, Appendix I). On the other hand, in the seven down-regulated DEPs, GO terms related to enzyme binding and activity were found as an enriched category when compared with the total of proteins identified (Fig. 6, Appendix I). These findings confirm that cyanobacterial biofilm development is closely associated with the up-regulation of the photosynthesis process.

The analysis of 41 DEPs found in this study is extremely important. Indeed, combining macroscopic evaluation of biofilm development with information about DEPs from proteomic analysis may provide new clues for mitigating marine biofouling. Since this study identified which proteins were down and up-regulated under different biofilms conditions, novel antifouling strategies which target these proteins can potentially be developed.

4. Conclusions

The present study, which presented several analyses, from the molecular to the macroscopic level, revealed the importance of combining different approaches to evaluate a complex phenomenon like biofilm formation. Based on macroscopic evaluation (biofilm biomass, thickness and chlorophyll *a* quantification), the results showed that hydrodynamic effects might be more important than surface properties in the development of cyanobacterial biofilms. However, on the proteomic approach, a large differential protein expression was found between biofilms formed on glass and perspex at 4 s^{-1}. New quantitative clues were provided to understand the diversity and function of proteins in cyanobacterial biofilm development. Combining all approaches applied in this study, the higher biofilm development at 4 s^{-1} may be related to up-regulation of SOD and differential expression of some uncharacterized proteins and proteins related to the photosynthetic process. On the other hand, the differential biofilm development observed on different surfaces is probably associated with different expression of a beta-propeller domain-containing protein, chaperone DnaK, SLH domain-containg proteins and/or an OMF family outer membrane protein and also the differential expression of some uncharacterized proteins on this cyanobacterial strain. Indeed, the fact that 50% of uncharacterized proteins found as DEPs in this study presented a disordered domain was a significant finding for cyanobacterial biofilm studies as these proteins represent complex systems that are specifically regulated by various means. Some of those uncharacterized proteins could be considered as a new relevant group of biofilm adaptation proteins since structural disorder can be beneficial for their resistance to environmental perturbations.

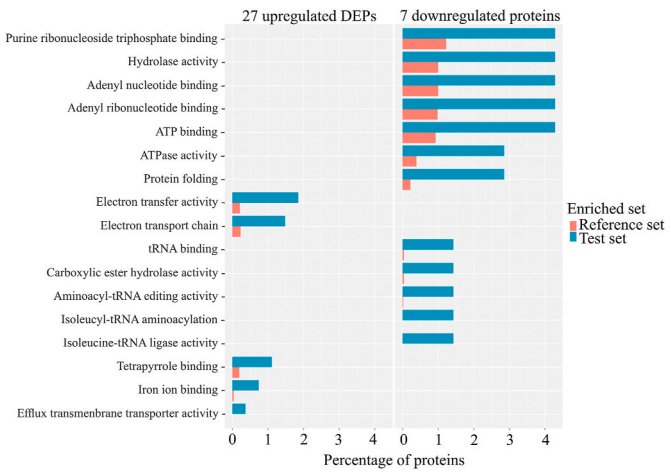

Fig. 6. Enrichment of DEPs revealed by the hypergeometric distribution significance test. The enriched GO terms (Fisher's exact test, $P < 0.05$) are represented by a stacked bar (in green) as the percentage of the GO terms found in the References Set (in red, represent all 546 identified). Each panel displays the set of 27 up-regulated and seven down-regulated DEPs found in the comparison glass *vs* perspex at 4 s^{-1}. More details about GO annotation can be found in the Appendix I. (For interpretation of the references to colour in this figure legend, the reader is referred to the Web version of this article.)

Advances in "omics" technologies are constantly evolving and their application to marine biofilm studies is an emerging approach that can lead to new improvements in antifouling strategies. Future studies should focus on different cyanobacterial strains, as well as evaluation of EPS secretion on these different biofilm conditions. Proteomic analysis should also be performed at different biofilm stages to evaluate differences in proteomic profile along biofilm formation and maturation. Moreover, different omics approaches, such as metabolomic studies, may be useful to identify additional pathways that can be involved in these biofilm development conditions. These further studies should also focus on cyanobacterial gene modifications or deletions, which encode relevant proteins reported in the present study as crucial for biofilm development to clarify their role on biofilm phenotypes.

Declaration of competing interest

The authors declare that they have no known competing financial interests or personal relationships that could have appeared to influence the work reported in this paper.

Acknowledgements

This work was financially supported by: Base Funding - UIDB/00511/2020 of the Laboratory for Process Engineering, Environment, Biotechnology and Energy – LEPABE - funded by national funds through the FCT/MCTES (PIDDAC), project HealthyWaters (NORTE-01-0145-FEDER-000069), supported by Norte Portugal Regional Operational Programme (NORTE 2020), under the PORTUGAL 2020 Partnership Agreement, through the European Regional Development Fund (ERDF) and strategic funding UIDB/04423/2020 and UIDP/04423/2020 through national funds provided by FCT and ERDF, in the framework of the programme PT2020. This work was also supported by the FCT project MOREBIVALVES (PTDC/ASP-PES/31762/2017) and it had support from the Portuguese Mass Spectrometry Network, integrated in the National Roadmap of Research Infrastructures of Strategic Relevance (ROTEIRO/0028/2013; LISBOA-01-0145-FEDER-022125). M.J. R. acknowledges a PhD grant from FCT (SFRH/BD/140080/2018).

Appendix A-J. Supplementary data

Supplementary data to this article can be found online at https://doi.org/10.1016/j.envres.2021.111566.

References

Agostoni, M., Waters, C.M., Montgomery, B.L., 2016. Regulation of biofilm formation and cellular buoyancy through modulating intracellular cyclic di-GMP levels in engineered cyanobacteria. Biotechnol. Bioeng. 113, 311–319. https://doi.org/10.1002/bit.25712.

Allen, R., Rittmann, B.E., Curtiss, R., 2019. Axenic biofilm formation and aggregation by *Synechocystis* PCC 6803 is induced by changes in nutrient concentration, and requires cell surface structures. Appl. Environ. Microbiol. 85, 1–33. https://doi.org/10.1101/414151.

Almeida, D., Domínguez-Pérez, D., Matos, A., Agüero-Chapin, G., Osório, H., Vasconcelos, V., Campos, A., Antunes, A., 2020. Putative antimicrobial peptides of the posterior salivary glands from the cephalopod *Octopus vulgaris* revealed by exploring a composite protein database. Antibiotics 9, 1–20. https://doi.org/10.3390/antibiotics9110757.

Babele, P.K., Kumar, J., Chaturvedi, V., 2019. Proteomic De-regulation in cyanobacteria in response to abiotic stresses. Front. Microbiol. 10, 1–22. https://doi.org/10.3389/fmicb.2019.01315.

Babele, P.K., Singh, G., Kumar, A., Tyagi, M.B., 2015. Induction and differential expression of certain novel proteins in *Anabaena* L31 under UV-B radiation stress. Front. Microbiol. 6, 1–14. https://doi.org/10.3389/fmicb.2015.00133.

Bakker, D.P., Van Der Plaats, A., Verkerke, G.J., Busscher, H.J., Van Der Mei, H.C., 2003. Comparison of velocity profiles for different flow chamber designs used in studies of microbial adhesion to surfaces. Appl. Environ. Microbiol. 69, 6280–6287. https://doi.org/10.1128/aem.69.10.6280-6287.2003.

Battchikova, N., Muth-Pawlak, D., Aro, E.M., 2018. Proteomics of cyanobacteria: current horizons. Curr. Opin. Biotechnol. 54, 65–71. https://doi.org/10.1016/j.copbio.2018.02.012.

Bharti, A., Velmourougane, K., Prasanna, R., 2017. Phototrophic biofilms: diversity, ecology and applications. J. Appl. Phycol. 29, 2729–2744. https://doi.org/10.1007/s10811-017-1172-9.

Bink, A., Vandenbosch, D., Coenye, T., Nelis, H., Cammue, B.P.A., Thevissen, K., 2011. Superoxide dismutases are involved in *Candida albicans* biofilm persistence against miconazole. Antimicrob. Agents Chemother. 55, 4033–4037. https://doi.org/10.1128/AAC.00280-11.

Blain, S., Guillou, J., Tréguer, P.J., Woerther, P., Delauney, L., Follenfant, E., Gontier, O., Hamon, M., Leilde, B., Mer, D., Cnrs, U.M.R., Nicolas, P., Mer, D., Cnrs, F.R., Copernic, P.N., 2004. High frequency monitoring of the coastal marine environment using the MAREL buoy. J. Environ. Monit. 6, 569–575. https://doi.org/10.1016/S0005-2728(89)80347-0.

Campbell, W.S., Laudenbach, D.E., 1995. Characterization of four superoxide dismutase genes from a filamentous cyanobacterium. J. Bacteriol. 177, 964–972. https://doi.org/10.1128/jb.177.4.964-972.1995.

Campos, A., Danielsson, G., Farinha, A.P., Kuruvilla, J., Warholm, P., Cristobal, S., 2016. Shotgun proteomics to unravel marine mussel (*Mytilus edulis*) response to long-term exposure to low salinity and propranolol in a Baltic Sea microcosm. J. Proteomics 137, 97–106. https://doi.org/10.1016/j.jprot.2016.01.010.

Carvalho, C.C.C.R., 2018. Marine biofilms: a successful microbial strategy with economic implications. Front. Mar. Sci. 5, 1–11. https://doi.org/10.3389/fmars.2018.00126.

Cense, A.W., Peeters, E.A., Gottenbos, B., Baaijens, F.P., Nuijs, A.M., van Dongen, M.E., 2006. Mechanical properties and failure of *Streptococcus mutans* biofilms, studied using amicroindentation device. J. Microbiol. Methods 67, 463–472. https://doi.org/10.1016/j.mimet.2006.04.02.

Cheng, S., Cetinkaya, M., Gräter, F., 2010. How sequence determines elasticity of disordered proteins. Biophys. J. 99, 3863–3869. https://doi.org/10.1016/j.bpj.2010.10.011.

Chorus, I., Cavalieri, M., 2000. Cyanobacteria and algae. In: Bartram, J., Rees, G. (Eds.), Monitoring Bathing Waters: A Practical Guide to the Design and Implementation of Assessments and Monitoring Programmes. World Health Organization Report. E & FN Spon, London and New York, pp. 219–271.

Dessau, R.B., Pipper, C.B., 2008. ["R"–project for statistical computing]. Ugeskr. Laeger 170, 328–330.

Domínguez -Pérez, D., Almeida, D., Wissing, J., Machado, A.M., Jänsch, L., Castro, L.F., Antunes, A., Castro, L.F., Vasconcelos, V., Campos, A., Cunha, I., 2021. Proteogenomic characterization of the cement and adhesive gland of the pelagic gooseneck barnacle *Lepas anatifera*. Int. J. Mol. Sci. 22, 3370. https://doi.org/10.3390/ijms22073370.

Domínguez -Pérez, D., Almeida, D., Wissing, J., Machado, A.M., Jänsch, L., Castro, L.F., Antunes, A., Vasconcelos, V., Campos, A., Cunha, I., 2020. The quantitative proteome of the cement and adhesive gland of the Pedunculate Barnacle, *Pollicipes pollicipes*. Int. J. Mol. Sci. 21, 2524. https://doi.org/10.3390/ijms21072524.

Ehrnsperger, M., Gräber, S., Gaestel, M., Buchner, J., 1997. Binding of non-native protein to Hsp25 during heat shock creates a reservoir of folding intermediates for reactivation. EMBO J. 16, 221–229. https://doi.org/10.1093/emboj/16.2.221.

Engelhardt, H., Peters, J., 1998. Structural research on surface layers: a focus on stability, surface layer homology domains, and surface layer-cell wall interactions. J. Struct. Biol. 124, 276–302. https://doi.org/10.1006/jsbi.1998.4070.

Enomoto, G., Nomura, R., Shimada, T., Win, N.N., Narikawa, R., Ikeuchi, M., 2014. Cyanobacteriochrome SesA is a diguanylate cyclase that induces cell aggregation in *Thermosynechococcus*. J. Biol. Chem. 289, 24801–24809. https://doi.org/10.1074/jbc.M114.583674.

Faria, S.I., Teixeira-Santos, R., Gomes, L.C., Silva, E.R., Morais, J., Vasconcelos, V., Mergulhão, F.J.M., 2020b. Experimental assessment of the performance of two marine coatings to curb biofilm formation of microfoulers. Coatings 10, 893. https://doi.org/10.3390/coatings10090893.

Faria, S.I., Teixeira-Santos, R., Morais, J., Vasconcelos, V., Mergulhão, F.J.M., 2021. The association between initial adhesion and cyanobacterial biofilm development. FEMS Microbiol. Ecol. 97 https://doi.org/10.1093/femsec/fiab052 fiab052.

Faria, S.I., Teixeira-Santos, R., Romeu, M.J., Morais, J., Vasconcelos, V., Mergulhão, F.J.M., 2020a. The relative importance of shear forces and surface hydrophobicity on biofilm formation by coccoid cyanobacteria. Polymers 12, 653. https://doi.org/10.3390/polym12030653.

Flemming, H.-C., Murthy, P.S., Venkatesan, R., Cooksey, K., 2009. Marine and Industrial Biofouling, Biofouling. Springer Berlin Heidelberg, Los Angeles, USA. https://doi.org/10.1007/978-3-540-69796-1.

Fu, J., Zong, G., Zhang, P., Gu, Y., Cao, G., 2018. Deletion of the β-Propeller protein gene Rv1057 reduces ESAT-6 secretion and intracellular growth of *Mycobacterium tuberculosis*. Curr. Microbiol. 75, 401–409. https://doi.org/10.1007/s00284-017-1394-8.

Gloag, E.S., Fabbri, S., Wozniak, D.J., Stoodley, P., 2020. Biofilm mechanics: implications in infection and survival. Biofilms 2. https://doi.org/10.1016/j.bioflm.2019.100017, 100017.

Harvey, K.L., Jarocki, V.M., Charles, I.G., Djordjevic, S.P., 2019. The diverse functional roles of elongation factor tu (Ef-tu) in microbial pathogenesis. Front. Microbiol. 10, 1–19. https://doi.org/10.3389/fmicb.2019.02351.

Haslbeck, M., Franzmann, T., Weinfurtner, D., Buchner, J., 2005. Some like it hot: the structure and function of small heat-shock proteins. Nat. Struct. Mol. Biol. 12, 842–846. https://doi.org/10.1038/nsmb993.

Hughes, C.S., Moggridge, S., Müller, T., Sorensen, P.H., Morin, G.B., Krijgsveld, J., 2019. Single-pot, solid-phase-enhanced sample preparation for proteomics experiments. Nat. Protoc. 14, 68–85. https://doi.org/10.1038/s41596-018-0082-x.

Janesch, B., Koerdt, A., Messner, P., Schäffer, C., 2013. The S-Layer Homology Domain-containing protein SlhA from *Paenibacillus alvei* CCM 2051T is important for swarming and biofilm formation. PLoS One 8, 1–17. https://doi.org/10.1371/journal.pone.0076566.

Kaneko, T., Sato, S., Kotani, H., Tanaka, A., Asamizu, E., Nakamura, Y., Miyajima, N., Hirosawa, M., Sugiura, M., Sasamoto, S., Kimura, T., Hosouchi, T., Matsuno, A., Muraki, A., Nakazaki, N., Naruo, K., Okumura, S., Shimpo, S., Takeuchi, C., Wada, T., Watanabe, A., Yamada, M., Yasuda, M., Tabata, S., 1996. Sequence analysis of the genome of the unicellular cyanobacterium *Synechocystis* sp. strain PCC6803. II. Sequence determination of the entire genome and assignment of potential protein-coding regions (supplement). DNA Res. 3, 185–209. https://doi.org/10.1093/dnares/3.3.185.

Kaus, K., Biester, A., Chupp, E., Lu, J., Visudharomn, C., Olson, R., 2019. The 1.9 Acrystal structure of the extracellular matrix protein Bap1 from *Vibrio cholerae* provides insights into bacterial biofilm adhesion. J. Biol. Chem. 294, 14499–14511. https://doi.org/10.1074/jbc.RA119.008335.

Kim, Y.H., Choi, Y., Oh, Y.Y., Ha, N.C., Song, J., 2018. Plant growth-promoting activity of beta-propeller protein YxaL secreted from *Bacillus velezensis* strain GH1-13. bioRxiv 1–29. https://doi.org/10.1101/471185.

King, R.K., Flick, G.J., Smith, S.A., Pierson, M.D., Boardman, G.D., Coale, C.W., 2006. Comparison of bacterial presence in biofilms on different materials commonly found

in recirculating aquaculture systems. J. Appl. Aquacult. 18, 79–88. https://doi.org/10.1300/J028v18n01.
Kotai, J., 1972. Instructions for the preparation of modified nutrient solution Z8 for algae. Blindern, Oslo Nor. Instit. Water Res. 11, 5.
Kurdrid, P., Senachak, J., Sirijuntarut, M., Yutthanasirikul, R., Phuengcharoen, P., Jeamton, W., Roytrakul, S., Cheevadhanarak, S., Hongsthong, A., 2011. Comparative analysis of the *Spirulina platensis* subcellular proteome in response to low- and high-temperature stresses: uncovering cross-talk of signaling components. Proteome Sci. 9, 39. https://doi.org/10.1186/1477-5956-9-39.
Leary, D.H., Li, R.W., Hamdan, L.J., Hervey, W.J., Lebedev, N., Wang, Z., Deschamps, J. R., Kusterbeck, A.W., Vora, G.J., 2014. Integrated metagenomic and metaproteomic analyses of marine biofilm communities. Biofouling 30, 1211–1223. https://doi.org/10.1080/08927014.2014.977267.
Liu, Z., Huang, Y., 2014. Advantages of proteins being disordered. Protein Sci. 3, 539–550. https://doi.org/10.1002/pro.2443.
López-Ochoa, J., Montes-García, J.F., Vázquez, C., Sánchez-Alonso, P., Pérez-Márquez, V. M., Blackall, P.J., Vaca, S., Negrete-Abascal, E., 2017. *Gallibacterium* elongation factor-Tu possesses amyloid-like protein characteristics, participates in cell adhesion, and is present in biofilms. J. Microbiol. 55, 745–752. https://doi.org/10.1007/s12275-017-7077-0.
Martins, J.C., Domínguez-Pérez, D., Azevedo, C., Braga, A.C., Costa, P.R., Osório, H., Vasconcelos, V., Campos, A., 2020. Molecular responses of mussel *Mytilus galloprovincialis* associated to accumulation and depuration of marine biotoxins okadaic acid and dinophysistoxin-1 revealed by shotgun proteomics. Front. Mar. Sci. 7, 1–15. https://doi.org/10.3389/fmars.2020.589822.
Matos, A., Domínguez-Pérez, D., Almeida, D., Aguëro-Chapin, G., Campos, A., Osório, H., Vasconcelos, V., Antunes, A., 2020. Shotgun proteomics of Ascidians Tunic gives new insights on host-microbe interactions by revealing diverse antimicrobial peptides. Mar. Drugs 18. https://doi.org/10.3390/md18070362.
Mieszkin, S., Callow, M.E., Callow, J.A., 2013. Interactions between microbial biofilms and marine fouling algae: a mini review. Biofouling 29, 1097–1113. https://doi.org/10.1080/08927014.2013.828712.
Minchin, D., Gollasch, S., 2003. Fouling and Ships' Hulls : How Changing Circumstances and Spawning Events May Result in the Spread of Exotic Species, vol. 19, pp. 111–122. https://doi.org/10.1080/0892701021000057891.
Mitchell, A.L., Attwood, T.K., Babbitt, P.C., Blum, M., Bork, P., Bridge, A., Brown, S.D., Chang, H.Y., El-Gebali, S., Fraser, M.I., Gough, J., Haft, D.R., Huang, H., Letunic, I., Lopez, R., Luciani, A., Madeira, F., Marchler-Bauer, A., Mi, H., Natale, D.A., Necci, M., Nuka, G., Orengo, C., Pandurangan, A.P., Paysan-Lafosse, T., Pesseat, S., Potter, S.C., Qureshi, M.A., Rawlings, N.D., Redaschi, N., Richardson, L.J., Rivoire, C., Salazar, G.A., Sangrador-Vegas, A., Sigrist, C.J.A., Sillitoe, I., Sutton, G. G., Thanki, N., Thomas, P.D., Tosatto, S.C.E., Yong, S.Y., Finn, R.D., 2019. InterPro in 2019: improving coverage, classification and access to protein sequence annotations. Nucleic Acids Res. 47, D351–D360. https://doi.org/10.1093/nar/gky1100.
Moreira, J.M.R., Gomes, L.C., Whitehead, K.A., Lynch, S., Tetlow, L.A., Mergulhão, F.J., 2017. Effect of surface conditioning with cellular extracts on *Escherichia coli* adhesion and initial biofilm formation. Food Bioprod. Process. 104, 1–12. https://doi.org/10.1016/j.fbp.2017.03.008.
Muthusamy, S., Lundin, D., Mamede Branca, R.M., Baltar, F., González, J.M., Lehtiö, J., Pinhassi, J., 2017. Comparative proteomics reveals signature metabolisms of exponentially growing and stationary phase marine bacteria. Environ. Microbiol. 19, 2301–2319. https://doi.org/10.1111/1462-2920.13725.
Najmuldeen, H., Alghamdi, R., Alghofaili, F., Yesilkaya, H., 2019. Functional assessment of microbial superoxide dismutase isozymes suggests a differential role for each isozyme. Free Radic. Biol. Med. 134, 215–228. https://doi.org/10.1016/j.freeradbiomed.2019.01.018.
Oliveira, P., Pinto, F., Pacheco, C.C., Mota, R., Tamagnini, P., 2015. HesF, an exoprotein required for filament adhesion and aggregation in *Anabaena* sp. PCC 7120. Environ. Microbiol. 17, 1631–1648. https://doi.org/10.1111/1462-2920.12600.
Osório, H., Silva, C., Ferreira, M., Gullo, I., Máximo, V., Barros, R., Mendonça, F., Oliveira, C., Carneiro, F., 2021. Proteomics analysis of gastric cancer patients with diabetes mellitus. J. Clin. Med. 10, 407. https://doi.org/10.3390/jcm10030407.
Ow, S.Y., Cardona, T., Taton, A., Magnuson, A., Lindblad, P., Stensjö, K., Wright, P.C., 2008. Quantitative shotgun proteomics of enriched heterocysts from *Nostoc* sp. PCC 7120 using 8-plex isobaric peptide tags. J. Proteome Res. 7, 1615–1628. https://doi.org/10.1021/pr700604v.
Panda, B., Basu, B., Acharya, C., Rajaram, H., Apte, S.K., 2017. Proteomic analysis reveals contrasting stress response to uranium in two nitrogen-fixing *Anabaena* strains, differentially tolerant to uranium. Aquat. Toxicol. 182, 205–213. https://doi.org/10.1016/j.aquatox.2016.12.002.
Pandey, S., Rai, R., Rai, L.C., 2012. Proteomics combines morphological, physiological and biochemical attributes to unravel the survival strategy of *Anabaena* sp. PCC7120 under arsenic stress. J. Proteomics 75, 921–937. https://doi.org/10.1016/j.jprot.2011.10.011.
Parnasa, R., Nagar, E., Sendersky, E., Reich, Z., Simkovsky, R., Golden, S., Schwarz, R., 2016. Small secreted proteins enable biofilm development in the cyanobacterium *Synechococcus elongatus*. Sci. Rep. 6, 1–10. https://doi.org/10.1038/srep32209.
Peterson, B.W., van der Mei, H.C., Sjollema, J., Busscher, H.J., Sharma, P.K., 2013. A distinguishable role of eDNA in the viscoelastic relaxation of biofilms. mBio 4. https://doi.org/10.1128/mBio.00497-13.
Porra, R., Thompson, W., Kriedemann, P., 1989. Determination of accurate extinction coefficients and simultaneous equations for assaying chlorophylls *a* and *b* extracted with four different solvents: verification of the concentration of chlorophyll standards by atomic absorption spectroscopy. Biochim. Biophys. Acta 975, 384–394. https://doi.org/10.1016/S0005-2728(89)80347-0.
Priya, B., Premanandh, J., Dhanalakshmi, R.T., Seethalakshmi, T., Uma, L., Prabaharan, D., Subramanian, G., 2007. Comparative analysis of cyanobacterial superoxide dismutases to discriminate canonical forms. BMC Genom. 8, 1–10. https://doi.org/10.1186/1471-2164-8-435.
Qayyum, S., Sharma, D., Bisht, D., Khan, A.U., 2016. Protein translation machinery holds a key for transition of planktonic cells to biofilm state in *Enterococcus faecalis*: a proteomic approach. Biochem. Biophys. Res. Commun. 474, 652–659. https://doi.org/10.1016/j.bbrc.2016.04.145.
Ramos, V., Morais, J., Castelo-Branco, R., Pinheiro, Â., Martins, J., Regueiras, A., Pereira, A.L., Lopes, V.R., Frazão, B., Gomes, D., Moreira, C., Costa, M.S., Brûle, S., Faustino, S., Martins, R., Saker, M., Osswald, J., Leão, P.N., Vasconcelos, V.M., 2018. Cyanobacterial diversity held in microbial biological resource centers as a biotechnological asset: the case study of the newly established LEGE culture collection. J. Appl. Phycol. 30, 1437–1451. https://doi.org/10.1007/s10811-017-1369-y.
Ritchie, M.E., Phipson, B., Wu, D., Hu, Y., Law, C.W., Shi, W., Smyth, G.K., 2015. Limma powers differential expression analyses for RNA-sequencing and microarray studies. Nucleic Acids Res. 43, e47. https://doi.org/10.1093/nar/gkv007.
Romeu, M.J., Alves, P., Morais, J., Miranda, J.M., de Jong, E.D., Sjollema, J., Ramos, V., Vasconcelos, V., Mergulhão, F.J.M., 2019. Biofilm formation behaviour of marine filamentous cyanobacterial strains in controlled hydrodynamic conditions. Environ. Microbiol. 21, 4411–4424. https://doi.org/10.1111/1462-2920.14807.
Romeu, M.J.L., Domínguez-Pérez, D., Almeida, D., Morais, J., Campos, A., Vasconcelos, V., Mergulhão, F.J.M., 2020. Characterization of planktonic and biofilm cells from two filamentous cyanobacteria using a shotgun proteomic approach. Biofouling 36, 631–645. https://doi.org/10.1080/08927014.2020.1795141.
Santos-Merino, M., Singh, A.K., Ducat, D.C., 2019. New applications of synthetic biology tools for cyanobacterial metabolic engineering. Front. Bioeng. Biotechnol. 7, 1–24. https://doi.org/10.3389/fbioe.2019.00033.
Shirkey, B., Kovarcik, D.P., Wright, D.J., Wilmoth, G., Prickett, T.F., Helm, R.F., Gregory, E.M., Potts, M., 2000. Active Fe-containing superoxide dismutase and abundant sodF mRNA in *Nostoc commune* (cyanobacteria) after years of desiccation. J. Bacteriol. 182, 189–197. https://doi.org/10.1128/JB.182.1.189-197.2000.
Silva, E.R., Tulcidas, A.V., Ferreira, O., Bayón, R., Igartua, A., Mendoza, G., Mergulhão, F.J.M., Faria, S.I., Gomes, L.C., Carvalho, S., Bordado, J.C.M., 2021. Assessment of the environmental compatibility and antifouling performance of an innovative biocidal and foul-release multifunctional marine coating. Environ. Res. 198, 111219. https://doi.org/10.1016/j.envres.2021.111219.
Sobczuk, T.M., Camacho, F.G., Grima, E.M., Chisti, Y., 2006. Effects of agitation on the microalgae *Phaeodactylum tricornutum* and *Porphyridium cruentum*. Bioproc. Biosyst. Eng. 28, 243–250. https://doi.org/10.1007/s00449-005-0030-3.
Stanier, R.Y., Cohen-Bazire, G., 1977. Phototrophic prokaryotes: the cyanobacteria. Annu. Rev. Microbiol. 31, 225–274. https://doi.org/10.1146/annurev.mi.31.100177.001301.
Sun, T., Li, S., Song, X., Diao, J., Chen, L., Zhang, W., 2018. Toolboxes for cyanobacteria: recent advances and future direction. Biotechnol. Adv. 36, 1293–1307. https://doi.org/10.1016/j.biotechadv.2018.04.007.
Suo, Y., Huang, Y., Liu, Y., Shi, C., Shi, X., 2012. The expression of superoxide dismutase (SOD) and a putative ABC transporter permease is inversely correlated during biofilm formation in *Listeria monocytogenes* 4b G. PLoS One 7, 1–9. https://doi.org/10.1371/journal.pone.0048467.
Taylor, D.A., 1996. Introduction to Marine Engineering. Butterworth-Heinemann. https://doi.org/10.1007/s11103-011-9767-z.Plastid.
Teodósio, J.S., Simões, M., Melo, L.F., Mergulhão, F.J.M., 2011. Flow cell hydrodynamics and their effects on *E. coli* biofilm formation under different nutrient conditions and turbulent flow. Biofouling 27, 1–11. https://doi.org/10.1080/08927014.2010.535206.
Terán, L.C., Distefano, M., Bellich, B., Petrosino, S., Bertoncin, P., Cescutti, P., Sblattero, D., 2020. Proteomic studies of the biofilm matrix including outer membrane vesicles of *Burkholderia multivorans* c1576, a strain of clinical importance for cystic fibrosis. Microorganisms 8, 1–18. https://doi.org/10.3390/microorganisms8111826.
Tomaras, A.P., Dorsey, C.W., Edelmann, R.E., Actis, L.A., 2003. Attachment to and biofilm formation on abiotic surfaces by *Acinetobacter baumannii*: involvement of a novel chaperone-usher pili assembly system. Microbiology 149, 3473–3484. https://doi.org/10.1099/mic.0.26541-0.
Trémoulet, F., Duché, O., Namane, A., Martinie, B., Labadie, J.C., 2002. Comparison of protein patterns of *Listeria monocytogenes* grown in biofilm or in planktonic mode by proteomic analysis. FEMS Microbiol. Lett. 210, 25–31. https://doi.org/10.1016/S0378-1097(02)00571-2.
Uversky, V.N., 2019. Intrinsically disordered proteins and their "Mysterious" (meta) physics. Front. Phys. 7 https://doi.org/10.3389/fphy.2019.00010.
Wagner, M., Horn, H., 2017. Optical coherence tomography in biofilm research: a comprehensive review. Biotechnol. Bioeng. 114, 1386–1402. https://doi.org/10.1002/bit.26283.
Wang, C., Lan, C.Q., 2018. Effects of shear stress on microalgae: a review. Biotechnol. Adv. 36, 986–1002. https://doi.org/10.1016/j.biotechadv.2018.03.001.
Wang, H., Yang, Y., Chen, W., Ding, L., Li, P., Zhao, X., Wang, X., Li, A., Bao, Q., 2013. Identification of differentially expressed proteins of *Arthrospira (Spirulina) plantensis*-YZ under salt-stress conditions by proteomics and qRT-PCR analysis. Proteome Sci. 11, 1. https://doi.org/10.1186/1477-5956-11-6.
Wang, X., Wang, C., Xu, B., Wei, J., Xiao, Y., Huang, F., 2018a. Adsorption of intrinsically disordered barnacle adhesive proteins on silica surface. Appl. Surf. Sci. 427, 942–949. https://doi.org/10.1016/j.apsusc.2017.08.108.

Wang, Y., Yi, L., Zhang, J., Sun, L., Wen, W., Zhang, C., Wang, S., 2018b. Functional analysis of superoxide dismutase of *Salmonella* typhimurium in serum resistance and biofilm formation. J. Appl. Microbiol. 125, 1526–1533. https://doi.org/10.1111/jam.14044.

Wiśniewski, J.R., Zougman, A., Nagaraj, N., Mann, M., 2009. Universal sample preparation method for proteome analysis. Nat. Methods 6, 359–362. https://doi.org/10.1038/nmeth.1322.

Yonezawa, H., Osaki, T., Woo, T., Kurata, S., Zaman, C., Hojo, F., Hanawa, T., Kato, S., Kamiya, S., 2011. Analysis of outer membrane vesicle protein involved in biofilm formation of *Helicobacter pylori*. Anaerobe 17, 388–390. https://doi.org/10.1016/j.anaerobe.2011.03.020.

Zhang, X., Smits, A.H., Van Tilburg, G.B.A., Ovaa, H., Huber, W., Vermeulen, M., 2018. Proteome-wide identification of ubiquitin interactions using UbIA-MS. Nat. Protoc. 13, 530–550. https://doi.org/10.1038/nprot.2017.147.

Zhao, W., Guo, Q., Zhao, J., 2007. A membrane-associated Mn-superoxide dismutase protects the photosynthetic apparatus and nitrogenase from oxidative damage in the cyanobacterium *Anabaena* sp. PCC 7120. Plant Cell Physiol. 48, 563–572. https://doi.org/10.1093/pcp/pcm025.

Zilliges, Y., Kehr, J.C., Mikkat, S., Bouchier, C., De Marsac, N.T., Börner, T., Dittmann, E., 2008. An extracellular glycoprotein is implicated in cell-cell contacts in the toxic cyanobacterium *Microcystis aeruginosa* PCC 7806. J. Bacteriol. 190, 2871–2879. https://doi.org/10.1128/JB.01867-07.